JOURNAL OF MATERIALS SCIENCE 27 (1992) 2110–2116

Laser shock on a TRIP alloy: mechanical and metallurgical consequences

D. GREVEY*, L. MAIFFREDY, A. B. VANNES‡
CALFETMAT – GEMPPM – INSA, 20 av. Albert Einstein, 69621 Villeurbanne Cedex, France

The present study concerns an Fe–Ni alloy (30% Ni) which was submitted to laser shocks with an energy density of 10^{15} and 10^{17} W m^{-2}. The main metallurgical consequence is the existence of a martensite transformation which appears in an area near to the back face of the sample. This was evidenced by microscopy and by measures of Vickers microhardness. The localization of the transformation can be explained by the reflection of the compression wave in the shape of an expansion wave. This study gives also, according to Meyer's theory, the maximum time necessary to induce the transformation, i.e. 40 ns. The mechanical consequence is the existence of tensile residual stresses at a level close to the strength limit. The stress field was determined by X-ray diffraction and by destructive methods. The shape of the stress field curve is quasi-sinusoidal with a period of about 150 mm; it is linked to the compression wave and to the expansion wave which follows the first one at the surface.

1. Introduction

Shock waves can be generated by different methods. The laser pulse is one of the more efficient methods (a great irradiance during a very short time, i.e. some nanoseconds) [1]. Pressures of 10 TPa during about 1 ns can be reached. Several effects of shock waves on metallic microstructure can be mentioned: important superficial cold-drawing, creation of internal stresses and even metallurgical transformations [2, 3], if the alloy composition makes it possible. In this study, we present these three effects on a well known Fe–Ni alloy [4]: this alloy with 30% Ni can be classified in the TRIP alloy steel family (TRansformation Induite par Plasticité–TRansformation Induced by Plasticity).

2. Experimental procedure

The laser had, mainly, a wavelength of 0.53 μm obtained by converting the initial wavelength with a KDP crystal. The total energy was 4000 J during 1 ns. The peripheral part of the target could be reached by the initial wavelength of 1.06 μm. The steel target composition is given in Table I.

The samples were prepared (for details see [5]) so that 30 mm diameter and 2 mm thick discs could be obtained. Homogeneity of the material was controlled by scanning-line secondary ion mass spectroscopy (SIMS) analysis in transverse section. Micrographic analysis revealed martensitic structure. The diameter of grains ranged between 30 and 70 μm. The martensitic start temperature M_s was determined as $-35.4\,^{\circ}C$ by microscopic observation during cooling of the sample.

The target was placed in a special test chamber. The shot conditions are summarized in Table II. Figs 1 and 2 described the visible effects of the shot on a target. Area No. 1 was illuminated by 0.53 μm wavelength whereas area No. 2 was illuminated by the losses due to 1.06 μm wavelength corresponding to two different loss energies of 15 and 25 J. In both samples, the diameter of the illuminated areas was 25 mm; the regions between 25 and 30 mm diameter of the target was not illuminated.

3. Results

3.1. Observations of the surface of sample No. 1011

The surface of sample 1011 was examined very carefully. The micrographs were divided as in Fig. 1. The central area showed "waves" of melted material; the distance between waves became progressively more constant as they moved away from the impact centre. In Fig. 3, the boundary between the area illuminated at 0.53 μm and that illuminated by the losses at 1.06 μm is shown. The strips of melted material are periodical in the vicinity of the impact side (Fig. 4). Sample 1013 had the same characteristics but on a different scale. Because of the cooling velocity, this melted layer would probably be microcrystalline. Fig. 5 shows twinned grains between the strips on sample 1011; details seen at higher magnification are presented in Fig. 6.

3.2. Observations on a transverse section of sample 1013

The transverse section surface was chemically etched by potassium metabisulphite [5]; observations by optical microscopy, SEM and TEM revealed three different areas along the depth as shown in Fig. 7.

* *Present address*: Laboratoire de Thermomécanique, Université de Bourgogne, 12 rue de la Fonderie, 71200 Le Creusot, France.
‡ *Present address*: Laboratoire Matériaux – Mécanique Physique, Route de Collonges, 69130 Ecully, France.

0022–2461

TABLE I Composition of the alloy (wt %)

Fe	Ni	Si	Mn	C	S	P
69.912	29.91	0.08	0.05	0.039	0.005	0.004

TABLE II Experimental conditions

Target No.	Fluence ($W\,cm^{-2}$)	Energy (J)	Focal spot diameter (mm)	Chamber pressure (Pa)
1011	10^{11}	625	25	5×10^{-4}
1013	10^{13}	1695	4.3	5×10^{-4}

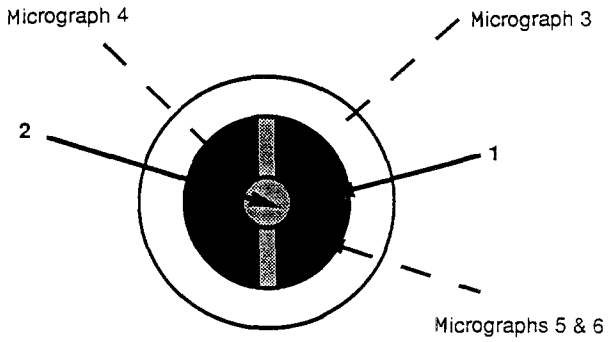

Figure 1 Illumination of sample No. 1011 at 0.53 μm (black areas) and 1.06 μm (shaded area).

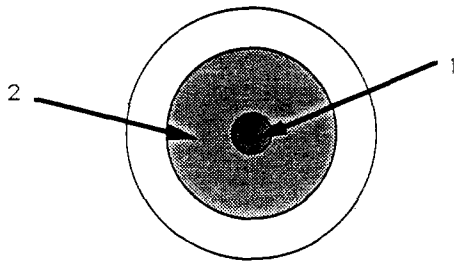

Figure 2 Illumination of sample No. 1013 at 0.53 μm (heavy shading) and 1.06 μm (light shading).

The first area close to the crater made by the laser shot, is about 30 μm thick. Its surface shows a wildly uneven topography. By TEM, very fine twinned crystals are seen in the grains at the surface and in the bulk (Fig. 8). This conforms to the observations of Figs 5 and 6. The second area affects nearly 1500 μm under the crater. Its main characteristic is to present a lot of twin crystals, so that, inside the grains, many families of twin crystals can exist.

The last 500 μm are different from the rest of the target because of the presence of martensite needles (Fig. 9). Finally, a non-transformed 70 μm thick area lies on the back face of the sample.

3.3. Hardness profiles

On sample 1013, two series of hardness tests were made:

(i) with 100 g load, an indentation size of nearly 30 μm is obtained, which is about the grain size (Fig. 10);

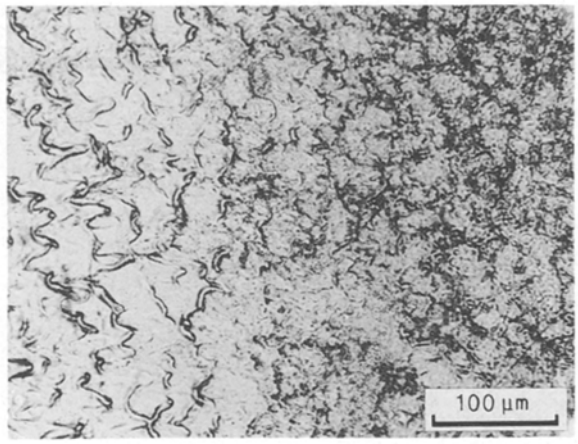

Figure 3 Boundary between areas 1 and 2 in sample 1011: area illuminated at 0.53 μm at left-hand side, area illuminated at 1.06 μm at right-hand side.

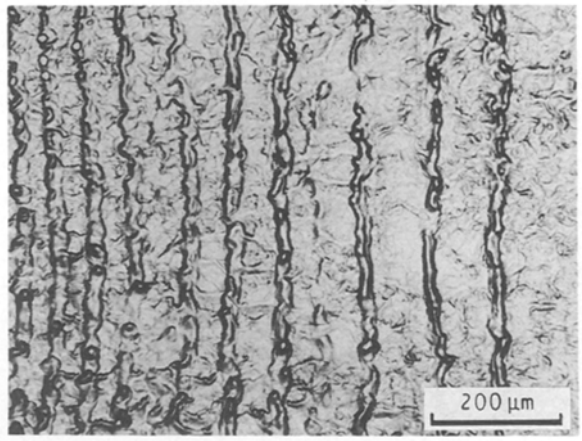

Figure 4 Evolution of the distance between the waves of the "melted" material.

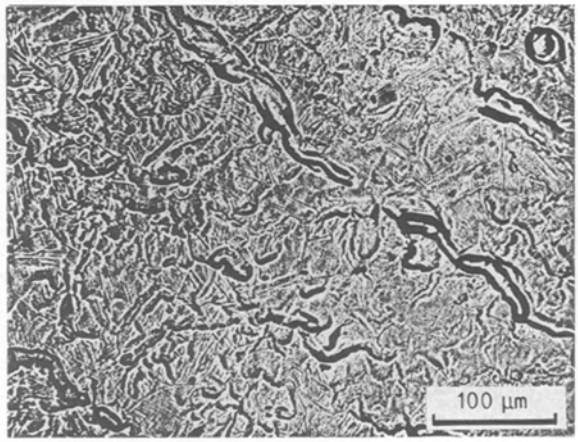

Figure 5 Twinned grains between the strips of the "melted" material.

(ii) with 10 g load the indentation size is a few micrometres so that a hardness graph with a step of 10 μm can be realized (Fig. 11).

Compared to the non-illuminated sample, an increase of hardness is obtained: 20 Vickers units under 10 g load and 10 Vickers units under 100 g load.

At a depth between nearly 1200 μm and 1600 μm, close to the face opposite to that of the impact, a twin

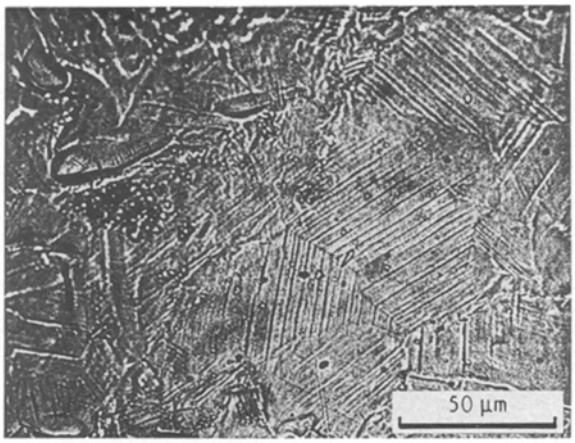

Figure 6 Detail of Fig. 5: twinned grains in the surface.

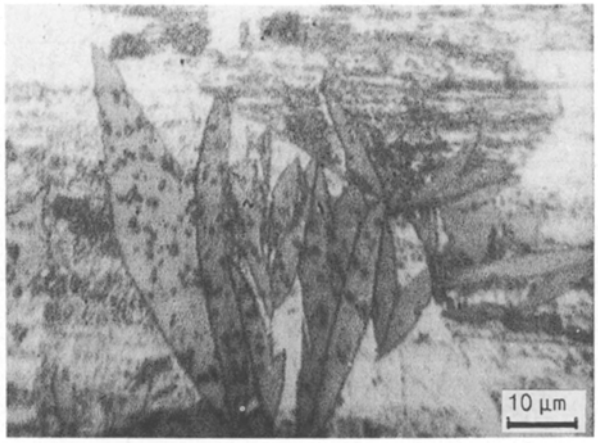

Figure 9 Needles of martensite (optical micrograph).

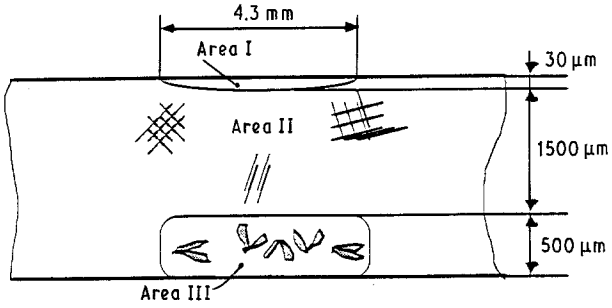

Figure 7 Schema of the cross-section of the three characteristic areas. Area I: very thin microstructure (twin crystals in some grains TEM). Area II: one or two twin crystal families in the grains. Area III: martensitic transformation in strips.

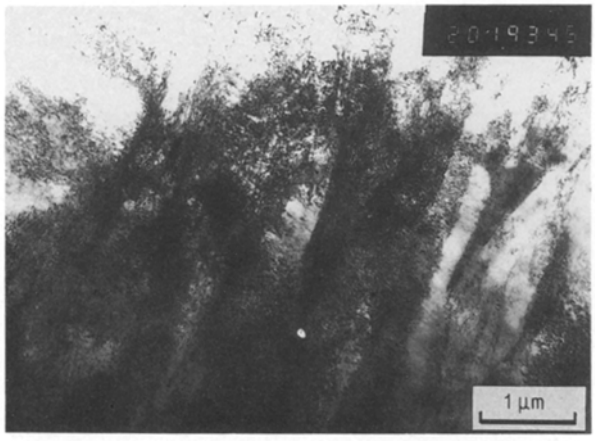

Figure 8 Twin crystals (TEM).

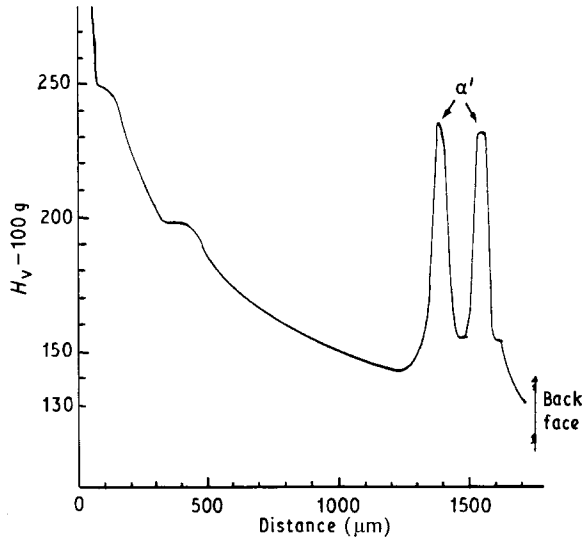

Figure 10 Vickers hardness under 100 g load: sample 1013.

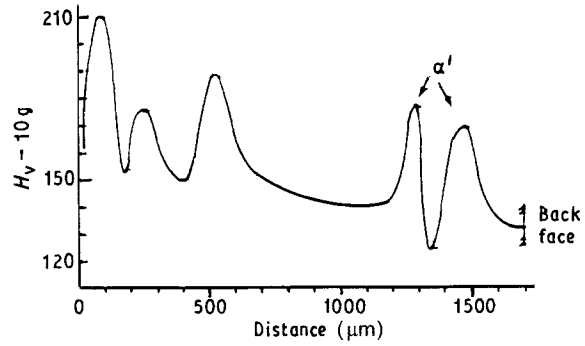

Figure 11 Vickers hardness under 10 g load: sample 1013.

hardness peak is in evidence. On the other hand, the curve shape of the first 600 µm is more disturbed under 10 g load than under 100 g load.

It can be noticed that the two hardness peaks close to the back face correspond to the area which is transformed to martensite. The hardness curve obtained under 10 g load reveals also that

(i) the first peak is related to the area with a lot of fine twin crystals;

(ii) the second one, at 250 µm depth, corresponds to the twin crystals visible by optical microscopy; and

(iii) the third one is probably due to a different grain orientation which would induce a greater local cold-drawing.

3.4. Residual stress determinations

The concept of residual stresses is based on elasticity theory. According to the point of view which is considered, different orders of stress can be distinguished [6, 7]. One is due to the elastic accommodation induced by the incompatibility of the deformations between some grains when cold drawing is achieved.

Equilibrium is reached in some grains. This concerns the second-order residual stresses, σ_{i2}. On the other hand, heterogeneities are induced by cold-drawing, on a macroscopic scale; they come from the elastic accommodation due to the absence of equilibrium of the second-order residual stresses from one area to another. These stresses are called first-order residual stresses, σ_{i1}.

3.4.1. Second-order residual stresses

Their determination is rather difficult. It is possible by measurement of the enlargement of the X-ray diffraction peaks [8, 9]. To a first approximation, the average stress is given by the simplified formula $\sigma_{i2} = E_{hkl}\ L_e/2\ \tan\ \theta_0$ where E_{hkl} = Young's modulus, L_e = X-ray peak width due to the cold drawing where $L_e = (L_t^2 - L_{nt}^2)^{1/2}$ and L_t = X-ray width before convolution treatment, L_{nt} = X-ray width after convolution treatment; θ_0 = Bragg angle.

In fact, in this expression the enlargement due to the change in the size of the crystallites is not taken into account. However, in this way an order of magnitude can be given. Considering the (2 2 0) reflection, the calculated value of the internal stress is about 650 MPa, using a Young's modulus of 180 GPa.

3.4.2. First-order residual stresses

Serveral methods can be used [10]. We chose two of them.

3.4.2.1. Superficial X-ray diffraction method

The X-ray diffraction $\sin^2 \psi$ method was used as usual [11, 12]. Because of the alloy composition, we used a manganese anticathode and the (3 1 1) peak. Seven incidence angles between -40 and $+45°$ were used and the results are summarized in Table III; we assumed a Young's modulus of 180 GPa and a Poisson's ratio $\nu = 0.29$. The surface of the reference sample 1000 was slightly under compressive stresses. Both illuminated samples were under tension. The order of magnitude of the stress is similar to that of the second order. This means that these two types of residual stress are close to the yield strength of the metal in the area considered.

TABLE III Residual stresses by the $\sin^2 \Psi$ method

Sample number	Measurement number	Main stresses (MPa)		
		σ_1	σ_2	σ_3
1000 (before treatment)	1	− 102	− 53	0
1011	1	592	554	− 1
	2	623	601	0
	3	211	191	0
1013	1	417	401	− 1
	2	440	605	− 4

3.4.2.2. Bulk method

The determination of the residual stress field as a function of depth was achieved using a method based on the removal of layers which was developed in our laboratory [13, 14]. The layers to be removed are very thin, so we designed and made a specific electrochemical machining cell; the machining conditions are close to those used for electrolytic polishing. To measure the thickness of the layer removed from the sample, we used an ultrasound apparatus working in reflection connected with a fast oscilloscope. Measurements of the strains were made every 10 μm and in two main perpendicular directions. Then, using an appropriated formalism [14], we were able to obtain the stress in every plane parallel to the impact surface. The residual stress field thus obtained is shown in Fig. 12. The variations of stress versus depth are nearly sinusoidal.

4. Discussion

From the experimental study of the sample, two important results were obtained:

(i) the existence of a martensitic transformation close to the back face of the sample, and

(ii) the shape of the residual stress field.

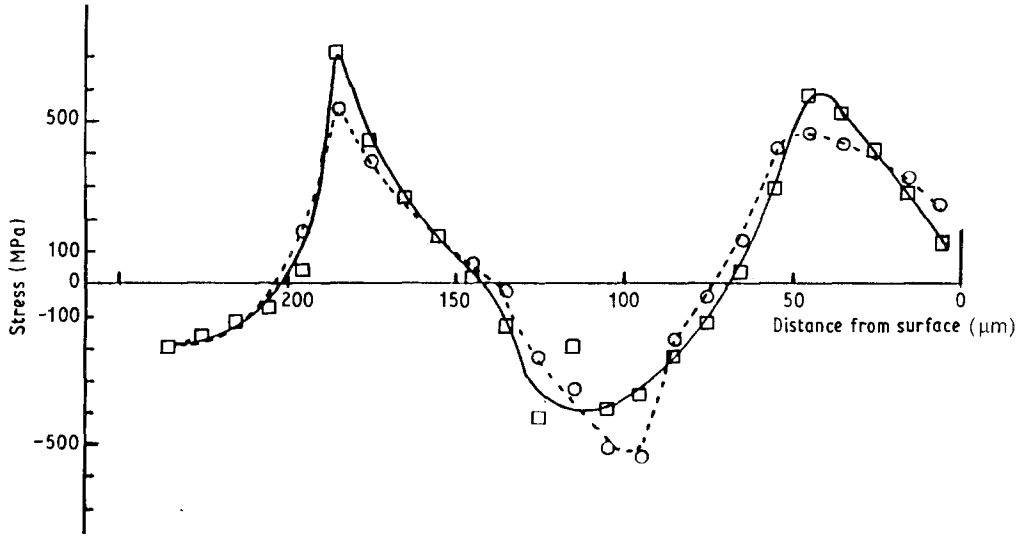

Figure 12 Residual stress field on sample 1011: (□) first gauge (σ_1), (○) second gauge at 90° (σ_2).

4.1. Metallurgical analysis

Very small twinned crystals were found just under the crater and at greater depth; this is in agreement with Mikkola's observations on copper and molybdenum [15]. The increase of hardness can be linked with the creation of a great density of dislocations. Loops of twin crystals appear after 10 ns interaction time. At the crater surface, twin crystals are related to the surface waves. Because of the laser–material interaction, the surface temperature increases to reach high values very quickly [11]. At the same time, thermodynamic non-equilibrium existing in the plasma induces strong compression waves across the material.

A thin superficial layer, acting like a viscous fluid, is deformed in a wavy shape. When the laser–material interaction is stopped the material is suddenly solidified, mainly because the target acts like a "thermal hole" so that the crater surface is distorted in waves and shows a very fine microstructure. The large size of the illuminated surface makes the observations easier.

In depth, the compression shock waves are probably responsible for cold-drawing and twinning. In Figs 10 and 11, the hardness peaks denote a heterogeneity of the deformation, which is related to the shock waves according to Meyers *et al.* [16]. Our observations seem to show an effect of the orientation of the grain with respect to the displacement of the waves. These grains, which are aligned in a strip, have a greater hardness than the adjacent ones. This is in agreement with the observations of Meyers [17], who showed that the shock impedance of the grains depended on their crystallographic orientation.

4.2. Analysis of the martensite transformation

Because of the composition of the alloy, the increase of volume which is a consequence of the transformation to martensite phase α' from the austenite phase γ has been estimated to be about 5%. The wave induced by the illumination of a 14 mm^2 surface during 1 ns with an energy of 1700 J is a compression wave; thus this wave cannot promote such a transformation. However, this wave is reflected at the back face of the sample leading to an expansion wave able to promote the transformation. Furthermore, as shown by Robin's work [4] using the Clausius–Clapeyron equation

$$\Delta H = T\frac{(\mathrm{d}P}{\mathrm{d}T_{\alpha\gamma})}\Delta V < 0$$

where ΔH is the enthalpy, $T_{\alpha\gamma}$ is the equilibrium temperature between the phases α and γ, and ΔV is the volume change. Hence an increase of the pressure P implies a decrease of $T_{\alpha\gamma}$ to keep ΔV positive. On the other hand, when ΔV is positive, decreasing P implies an increase of $T_{\alpha\gamma}$. Meyers [18] notes that the effect of pressure is to increase the M_s temperature by about 83 K per GPa (in the range of temperature M_s–M_d in which the martensitic transformation is possible), when there is no heating of the back face of the sample.

So, existence of the martensite transformation implies (in the area of the sample considered) that the M_s point was increased to a temperature at least equal to the room temperature; hence, because of an initial M_s point of $-35\,^{\circ}C$, the pressure would be about 0.6 GPa. This is quite possible with our experimental conditions. However, two points have to be clarified:

(i) the transformation in strips can be linked to the hypothesis of the previous part. Morin [19] showed that the transformation starts close to the structure defects, which corroborates our approach,

(ii) the position and the nucleation time.

Different opinions about the germination mechanism of the martensite have been presented. The nucleation time of martensite can be estimated according to Meyers' theory as the duration during which the pressure has to be effective to allow the transformation, if the wave front is rectangular and if the velocities of expansion and compression waves are equal. This is about 40 ns with our experimental conditions; hence we can conclude that the incubation time, if it exists, is less than 40 ns.

Other people argue on the basis of one thermal activation or of a mechanical instability and do not speak about nucleation time, but use the notion of "instantaneity". This notion lies, in fact, on a microsecond scale and is hence much greater than 40 ns, so there is no discrepancy with these theories.

4.3. Residual stresses

Hardening technologies involving superficial work-hardening, shot-peening for example, induce compressive residual stresses in external layers. In contrast, with laser treatment, measurements by X-ray diffraction and by destructive methods show tensile residual stresses at a significant level close to the strength limit. Other measurements, performed in other laboratories, point to compressive residual stresses when the created plasma is confined [20]. However, analysis of the stress field shows (Fig. 12) a nearly sinusoidal distribution with a period of about 150 μm. Analysis of the stress field can be established using a block diagram [9]. There is no doubt that the shock wave induces a differential work hardening. We discuss in terms of equivalent strain in a single direction. This simplification can be accepted because our approach is only qualitative.

To simplify, let us consider that our sample is divided along its thickness into two blocks (Fig. 13).

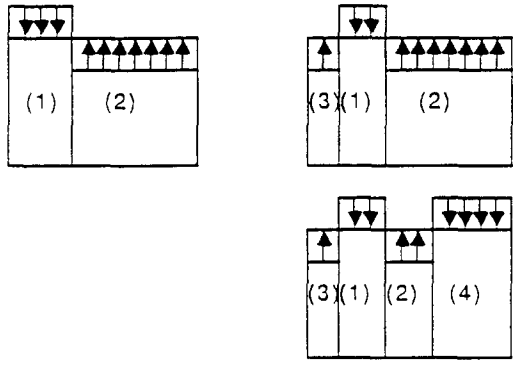

Figure 13 Block diagrams illustrating the obtained internal stress field (for explanation see text).

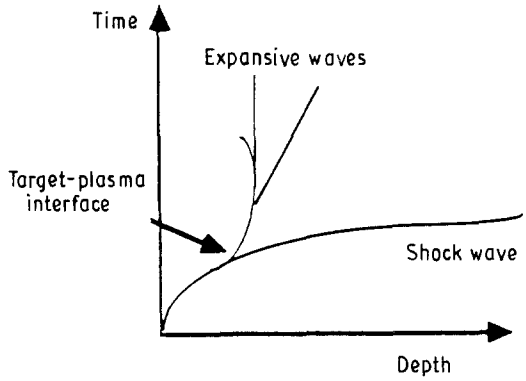

Figure 14 Evolution time versus depth of the waves.

The shot-peening shape implies a 150 μm thick block 1, near the impact. It is dilated compared to block 2 which is less work-hardened. Now, the necessary continuity between the two blocks requires the first one to be under compression and the second one to be under tension.

This is in disagreement with the results obtained. Nevertheless, the convergent beam of compressive waves, created at the target surface, induces a shock wave inside the material, and is always followed by a divergent beam of expansive waves. This divergence implies that the second beam is effective only on a small thickness. These processes are qualitatively described in Fig. 14. The expansive wave would induce a localized relaxation by work-hardening in an opposite direction, which would create block 3 in Fig. 13. If this approach is correct, it can be asserted that the phenomenon occurs over a thickness of about 60 μm.

The second period can be explained by the natural crossing of block 1 in compression to block 2 which is consequently in tension, because of the work-hardening difference induced by the first compression wave. Then block 4 has a stress level approximatively equal to that measured on the untreated sample.

The reasons why compressive stresses appear when the plasma is confined [20] could be that the effects of the expansive waves are annihilated by the thermal effects. Plasma confinement increases its temperature by 1 to 2 orders of magnitude. To confirm this explanation, some experiments similar to ours would be necessary.

5. Conclusions

An Fe–Ni alloy or TRIP alloy (30% Ni) was submitted to a laser shock with an energy density of $10^{15}\,W\,m^{-2}$ ($10^{11}\,W\,cm^{-2}$) and $10^{17}\,W\,m^{-2}$ ($10^{13}\,W\,cm^{-2}$). The shock waves, due to the effect of plasticity, induce a martensitic transformation; this is localized close to the back face of the sample and seems to be due not to the initial compression wave but to the expansion wave, which is the wave reflected from the back face. The necessary time of application of the pressure can be estimated to be about 40 ns. According to Meyers' theory, this duration would be the maximum duration necessary to induce this transformation.

The hardness evolution versus depth is linked, just under the crater surface, to the defects created by the crossing of the compressive wave, and, near the back face, with the martensite transformation.

The residual stresses induced by this kind of treatment were determined as follows:

(i) Using X-ray diffraction, tensile residual stresses were detected on the illuminated surface at a level superior to 600 MPa, i.e. very close to the strength limit of this material.

(ii) Using a destructive method, by electrolytic removal of layers, a nearly sinusoidal variation of the residual stress field versus depth was determined with a period of about 120–150 μm and with a level similar to that measured by the X-ray diffraction method. The first period can be linked to the compression wave and the expansion wave which follows the first one at the surface; the second can be explained by the accommodation between, on the one hand, the first 150 μm hardly affected by the compression and expansion wave, and, on the other hand, the rest of the sample which was initially lightly compressed.

This work allowed us to understand the phenomena which occur in the bulk of the sample. Nevertheless, some questions remain:

(i) Concerning the residual stresses: changing the conditions to create a laser shock and the durations of the waves, a detailed analysis of the different residual stress fields could explain the variations, and in particular the reason why, when there is confinement, the residual stresses in the surface are in compression.

(ii) Concerning the martensite transformation: it is necessary to improve our results by experiments of the same kind as those made for the residual stress study.

Acknowledgements

The authors would like to thank Professor Maeder and Dr Lebrun for their aid in the measurements of residual stresses by the $\sin^2\psi$ method.

References

1. R. M. WHITE, *J. Appl. Phys.* **34** (1963) 2123.
2. D. W. GREGG and S. J. THOMAS, *ibid.* **37** (1966) 2787.
3. M. A. MEYERS, *Scripta Metall.* **12** (1978) 21.
4. M. ROBIN Thèse Sci. INSA de Lyon (1981).
5. D. GREVEY, Thèse Sci. INSA de Lyon (1988).
6. E. MACHERAUCH, H. WOHLFAHRT and U. WULFSTIEG, *Härterei-Technische Mitteilungen* No. 28 (1973).
7. A. B. VANNES, R. FOUGERES and M. THEOLIER, *Rev. Traitement Thermique* No. 87 (1974) 67.
8. A. GUINIER "Thèorie et technique de la radiocristallographie", Dunod, Paris (1956).
9. A. B. VANNES, Thèse Sci. INSA de Lyon (1978).
10. M. PILLOZ, Thèse Sci. INSA de Lyon (1990).
11. F. LECROISEY, B. MIEGE and E. SAINT-ETIENNE, "La mesure des contraintes résiduelles. Méthode de détermination par rayons X", Mémoires Techniques du CETIM No. 33 (CETIM, Senlis, 1978).
12. G. MAEDER, J. L. LEBRUN and J. M. SPAUEL, *Matér. Techn.* No. 4/5 (1981) 135.
13. J. HERNANDEZ, T. LATCHI, M. P. GENCE, C. BIGNON, M. BONIN, M. LARACINE, M. LORMAND and A. B. VANNES, *Mécan. Matér. Electr.* No. 415 (1986) 58.
14. A. B. VANNES, "Détermination et influence des contraintes résiduelles par enlèvement de matière: méthodes destructives" (Cast, Lyon, 1977).

15. D. E. MIKKOLA, "Effects of Shock Loading Variables on Shock-wave Strengthening of Metals", N79 23204 (Michigan Technological University, Houghton, 1979).
16. M. A. MEYERS, N. N. THADANI, D. C. ERLHICH and P. S. DECARLI, in "Shock Waves in Condensed Matter" edited by J. R. Aday, R. A. Graham and G. K. Straub (Elsevier Science, New York, 1984) pp. 411–414.
17. M. A. MEYERS, In Proceedings of 5th International Conference on High Energy Rate Fabrication, University of Denver, Colorado, June 1985 (Denver Research Inst.) pp. 141–161.
18. *Idem., Metall. Trans. A* **10** (1979) 1723.
19. M. MORIN, Thèse Sci. INSA de Lyon (1985).
20. J. FOURNIER, Thèse Physique, Ecole Polytechnique, Paris (1989).

Received 17 December 1990
and accepted 13 May 1991